Biophysical Journal, Volume 99

Supporting Material

Hydrodynamics of Sperm Cells near Surfaces

Jens Elgeti, U. Benjamin Kaupp, and Gerhard Gompper

Hydrodynamics of Sperm Cells near Surfaces

Jens Elgeti, U. Benjamin Kaupp, and Gerhard Gompper

Supporting Material

I. SPERM MODEL

The flagellum is modeled as a crane-like structure shown in Fig. 1. Three semi-flexible rods, each consisting of $N_f = 100$ monomers of mass M, are arranged in a filamentous structure with a triangular cross section.

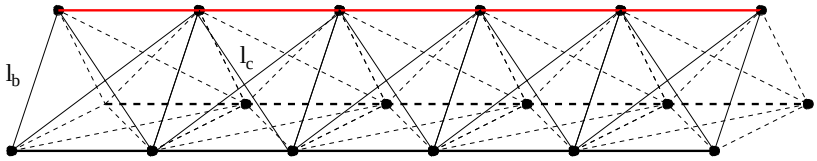

FIG. 1: The flagellum is modeled as three semi-flexible filaments that are connected by harmonic springs of length ℓ_b (nearest neighbors) and ℓ_c (next-nearest neighbors) to form a crane-like structure. Bond lengths on the top filament (red) are varied to induce both dynamic and static bending.

The bond length ℓ_b between neighboring monomers and the distance between the parallel filaments are identical. The filament length is kept nearly constant by a strong harmonic potential

$$U = \frac{1}{2} K_1 (|\Delta \mathbf{r}_i| - \ell_b)^2, \tag{1}$$

between neighboring monomers, with spring constant K_1, where $\Delta \mathbf{r}_i = \mathbf{r}_{i+1} - \mathbf{r}_i$ are the bond vectors. The bending stiffness of each filament is described by a curvature potential,

$$U = -K_b \sum_i \Delta \mathbf{r}_i \cdot \Delta \mathbf{r}_{i+1} \tag{2}$$

with bending rigidity K_b. The filaments are connected by harmonic springs between nearest-neighbor (bond length ℓ_b, spring constant K_1) and next-nearest-neighbor (bond length $\ell_c = \sqrt{2}\ell_b$, spring constant K_2) monomers with an interaction potential analogous to Eq. (1). All spring constants are chosen much larger than the thermal energy $k_B T$, so that the mean-squared thermal fluctuations of the bond length are much smaller than the bond length itself. More specifically, we chose the parameters $M/m = 5$, $K_1 = 50\,000\, k_B T/\ell_b^2$, and

$K_2 = 5\,000\,k_BT/\ell_b^2$ (elastic tail) or $K_2 = 50\,000\,k_BT/\ell_b^2$ (stiff tail), and $K_b = 500 k_BT/\ell_b^2$. A similar model has been employed to model the rotating helical flagellum of swimming bacteria [1].

We determine the bending rigidity κ and the torsional rigidity J (assuming an elastic energy $E = 1/2\ J\Theta^2$ with torsion angle Θ) of the flagellum by calculating the energy for the corresponding deformations. With the chosen interaction parameters, the flagellum adopts an effective bending rigidity of $\kappa/L_f \approx 130 k_BT$ and a torsional rigidity $J \simeq 10 k_BT$ to $J \simeq 100 k_BT$ for elastic and stiff tails, respectively.

II. MULTI-PARTICLE COLLISION DYNAMICS: PARAMETERS AND BOUNDARY CONDITIONS

In our multi-particle collision dynamics (MPC) simulations, appropriate length and time scales of the sperm motion and of the fluid have to be chosen for three reasons: to achieve low-Reynolds-number hydrodynamics, slow diffusion compared to swimming, and good computational efficiency. We use the parameters $\lambda/a = 0.05$ (mean free path), $\alpha = 130^o$ (collision angle) and $\rho a^3 = 10$ (number density of fluid particles). These parameters yield a viscosity $\eta = 16.4\sqrt{mk_BT}/a^2$. For driven systems and for systems containing active swimmers, a global thermostat is used to keep the temperature constant. With a short bond length $\ell_b = 0.5\,a$, the flagellum, embedded in the MPC fluid, behaves hydrodynamically like a slender rod [2], see Sec. III.

To implement no-slip boundary conditions at the wall, we employ a combination of bounce-back scattering of fluid particles at the wall during the streaming step (*i.e.* $\mathbf{v} \to -\mathbf{v}$ for all particles hitting the wall) and virtual wall particles, which participate in the collision step for all collision cells overlapping with the wall. This method has been shown to approximate no-slip boundary conditions very well [3], and is commonly employed [4].

In the resistive-force simulations, all monomers of head and flagellum interact with the wall via a short-ranged Lennard-Jones potential, with an interaction range $\sigma = \ell_b/2$.

For the simulations of sperm swimming in the bulk, we employ a cubic simulation box of linear size $S = 70\,a$. For the simulation of sperm motion near walls, we use a wall distance of $d = 50\,a$, with lateral size $75\,a \times 75\,a$. The wall distance equals the sperm length, which is comparable to typical experimental situations [5].

III. HYDRODYNAMICS OF SLENDER RODS IN MPC FLUIDS IN THE BULK

The flagellum behaves hydrodynamically like a slender, flexible rod [6]. In order to verify that our model, consisting of three connected filaments, properly reproduces the hydrodynamic properties of the flagellum, we determine the drag coefficients of the passive structure with orientation parallel and perpendicular to the direction of motion, and compare with analytical expressions [7] obtained from Stokes hydrodynamics.

Thin rods in a fluid have anisotropic friction coefficients, where the friction force perpendicular to the rod, $\vec{F}_\perp$ is larger then parallel, $\vec{F}_\parallel$. We define the drag coefficients of a rod in Stokes flow by

$$F_\parallel = \gamma_\parallel v_\parallel \quad , \quad F_\perp = \gamma_\perp v_\perp \tag{3}$$

with the subscripts $\parallel$, $\perp$ denote the vector components parallel and perpendicular to the rod, respectively. These friction coefficients are related to the diffusion coefficients $D_{\parallel,\perp}$ via the Stokes-Einstein relation

$$\gamma_{\parallel,\perp} = \frac{k_B T}{D_{\parallel,\perp}} \tag{4}$$

It has not been possible so far to derive exact analytical results for the diffusion coefficients of slender rods of finite length, but approximate expressions are available. Tirado, Martinez and de la Torre [7] review some theoretical approaches. The different theories agree on a logarithmic dependence on the aspect ratio,

$$\frac{2\pi\eta L_r D_\parallel}{k_B T} = \ln(L_r/d_r) + \nu_\parallel \tag{5}$$

$$\frac{4\pi\eta L_r D_\perp}{k_B T} = \ln(L_r/d_r) + \nu_\perp. \tag{6}$$

where L_r is the rod length, and d_r the rod diameter. Differences between theories are found concerning the correction functions $\nu_{\perp/\parallel}$. A often-used approximation for $2 < L_r/d_r < 30$ is

$$\nu_\parallel = -0.207 + 0.980 d_r/L_r - 0.133\,(d_r/L_r)^2 \tag{7}$$

$$\nu_\perp = 0.839 + 0.185 d_r/L_r + 0.233\,(d_r/L_r)^2 \ . \tag{8}$$

To compare these results of slender body theory to those of mesoscale hydrodynamics, we perform simulations to calculate $\gamma_\perp$ and $\gamma_\parallel$ of the connected three-filament structure in an MPC fluid, as explained in Ref. [2]. For this purpose, the flagellum structure is localized in

the center of a simulation box by a harmonic potential, and exposed to a constant flow. A uniform flow field is imposed sufficiently far from the rod by assigning Maxwell Boltzmann-distributed velocities, with an additional average velocity $\bar{v}$ in the flow direction, to the solvent particles in a layer of thickness a perpendicular to the flow direction. The friction coefficients are determined by a calculation of the drag forces. The drag force is found to be linear with $\bar{v}$ at least up to $\bar{v} \approx 0.3\sqrt{k_B T/m}$. We chose $\bar{v} = 0.1\sqrt{k_B T/m}$, well within the linear regime for the remaining simulations.

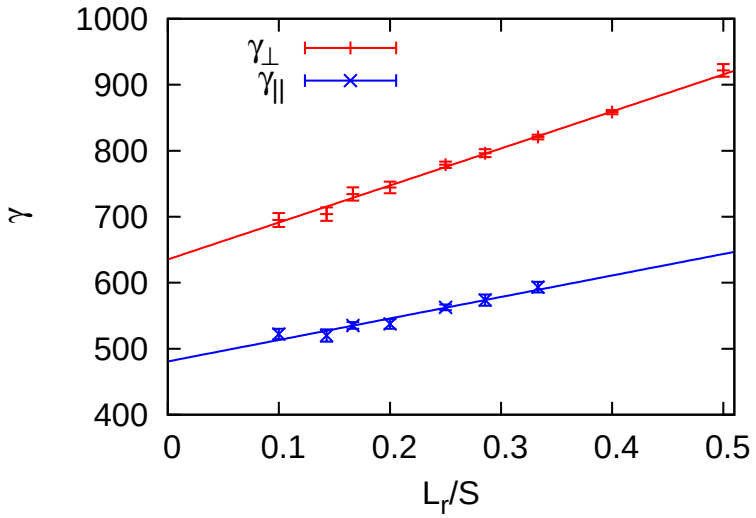

FIG. 2: Friction coefficients $\gamma_{\parallel}$ and $\gamma_{\perp}$ (in units of $(k_B T m/a^2)^{1/2}$) as a function of scaled inverse linear system size L_r/S. System size varies between $S = 20\,a$ and $S = 100\,a$. Rod length is $L_r = 10\,a$.

Fig. 2 shows as an example the friction coefficients $\gamma_{\parallel}$ and $\gamma_{\perp}$ as a function of scaled inverse linear system size L_r/S. To determine the friction coefficients at infinite dilution, we fit a linear function to the data (see Fig. 2), and used the extrapolation to infinite system size. The strong finite-size effects require large systems and limit the range of accessible rod lengths. The largest simulated systems used are for rods with length $L_r = 20\,a$ with $S = 110\,a$, corresponding to 13 million MPC particles.

Fig. 3 shows that the agreement of simulations and theory is very good, and the logarithmic divergence with rod length is well reproduced [2]. The fit of $\gamma_{\parallel}$ and $\gamma_{\perp}$ in Fig. 3 results in a rod diameter of $d_r \approx 0.9\,a$. This is a very reasonable result, given the fact that MPC cannot reproduce hydrodynamics on length scales smaller than the size a of a collision cell.

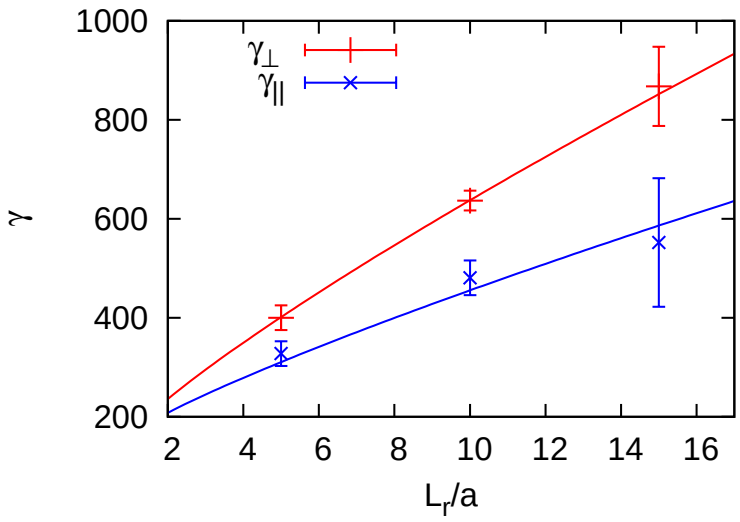

FIG. 3: Friction coefficients $\gamma_{\parallel}$ and $\gamma_{\perp}$ (in units of $(k_BTm/a^2)^{1/2}$) as a function of rod length L_r. The solid line is a fit of the theory (Eqs. (5) and (6)) to the data of $\gamma_{\perp}$, resulting in $d_r \approx 0.9\,a$. This value was then also used to plot $\gamma_{\parallel}$. Points are results of finite-size fits, as described in the text.

This result is also in good agreement with earlier simulation results for the total diffusion coefficient of a rod [8].

The sperm flagellum has a diameter of $0.3\mu m$, the typical sperm lengths are in the range of $30\mu m$ to $60\mu m$, so that sperm tails have characteristic aspect ratios $L_r/d_r \simeq 100\ldots200$. For such relatively small aspect ratios, Eqs. (5), (6) together with Eqs. (7), (8) imply $\gamma_{\perp}/\gamma_{\parallel} = 2[\ln(L_r/d_r) - 0.207]/[\ln(L_r/d_r) + 0.839]$, which leads to friction anisotropies $\gamma_{\perp}/\gamma_{\parallel} = 1.61\ldots1.66$, smaller than 2, consistent with earlier observations [6, 9, 10]. For the aspect ratio $L_r/d_r \approx 50$ of our sperm model, the theoretical estimate implies $\gamma_{\perp}/\gamma_{\parallel} = 1.56$. Thus, we use a friction anisotropy $\gamma_{\perp}/\gamma_{\parallel} = 1.5$ in our resistive-force simulations.

IV. SPERM MOTION – SWIMMING VERSUS DIFFUSION

A sperm cell is a micrometer-size object, and therefore displays Brownian motion – both without an with active beat of the flagellum. An estimate of the total diffusion constant $D = (D_{\parallel} + 2D_{\perp})/3$, can now be obtained easily by using the results of Sec. III, which imply

$$D = \frac{k_BT}{3\pi\eta L_r}\,[\ln(L_r/d_r) + 0.316] \tag{9}$$

For a the diffusion of rod-like particles of the length L_f of the flagellum ($L_f/d_f \simeq 50$) in a MPC fluid with viscosity $\eta = 16.4\sqrt{mk_BT}/a^2$, this provides the diffusion constant $D \simeq 10^{-4}a\sqrt{k_BT/m}$. The swimming velocity of a sperm is $v \simeq 0.0034\,\omega L_f = 0.017\sqrt{k_BT/m}$ for beat frequency $\omega = 0.1\sqrt{k_BT/ma^2}$. With these parameters, the time needed to swim a distance $L_f/2$ is about three orders of magnitude less than that needed by diffusion. Thus, swimming strongly dominates diffusion in our simulations.

V. HYDRODYNAMICS OF SLENDER RODS IN MPC FLUIDS NEAR SURFACES

Next, we verify the proper hydrodynamics of the flagellum beating near a plane wall. We consider a rod which is dragged parallel to a wall at a constant distance h, with the force perpendicular to the rod orientation.

The hydrodynamics of rods near walls has been studied within the Stokes approximation in Ref. [11], and analytical expressions for the drag force have been derived. For a rod of radius r pulled at constant velocity U, the drag force F_x per unit length was obtained to be [11]

$$F_x/L_r = -4\pi\eta U/\ln\left[\{h + (h^2 - r^2)^{1/2}\}/r\right] \tag{10}$$

where h the distance of the rod axis from the wall. This result applies in the limit $L_r \gg h$.

Similar to our simulations for the drag coefficients in the bulk, each monomer of a rod of length L, with an orientation in the y-direction, is confined by a harmonic potential

$$V(x,z) = V_0\left[(x - Ut)^2 + (y - y_0)^2 + (z - h)^2\right] \tag{11}$$

where h is the distance from a no-slip wall (at $z = 0$), and y_0 is the initial monomer position. The potential strength is $V_0 = 3.125\,k_BT/\ell_b^2$. Due to the strong bond potentials, which keep bond lengths essentially constant, the is equivalent to a harmonic potential for the center-line of the rod. To mimic an infinitely long rod, we apply periodic boundary conditions in x and y directions with a simulation box size $S_x = S_y = S = L$. A second no slip wall is located at $S_z = S$.

The potential is moved at a constant velocity of $U = 0.02\sqrt{k_BT/m}$ in the x direction. The no-slip boundary conditions with the wall at $z = 0$ cause the flow field to decay quickly in the

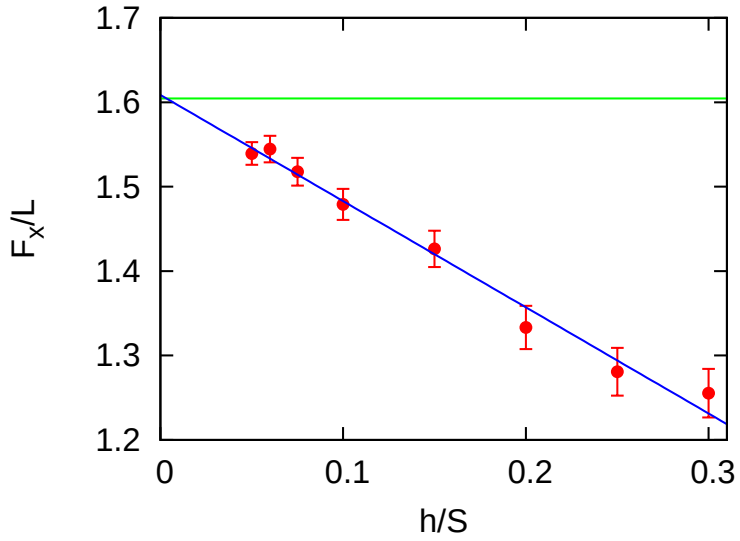

FIG. 4: Drag force F_x/L per unit length (in units of k_BT/a^2), for velocity $U = 0.02\sqrt{k_BT/m}$, at distance $h = 3a$ from a plane wall with no-slip boundary conditions, as a function of the scaled inverse system size h/S. Symbols (red) show simulation data, the green solid line the expected theoretical value, and the blue solid line the finite-size extrapolation. We estimate an error of the extrapolated value of about 3%.

direction parallel to the wall. Nevertheless, finite-size effects are observed. We extrapolate to infinite system size by assuming a h/S dependence, as shown in Fig. 4.

The resulting drag force F_x/L as a function of the distance from the wall is shown in Fig. 5. The simulation results show excellent agreement with the theoretical expression (10) for $h \gtrsim 2a$, without any adjustable parameters. For smaller distances, the friction coefficient continues to increase, but more weakly than the logarithmic divergence predicted by Eq. (10). Note that no numerical instabilities occur.

We want to mention parenthetically that very good agreement of near-wall hydrodynamics was obtained for rotating cylindrical colloids [12] and for translating spherical and rod-like colloids [13] embedded in an MPC fluid.

Because in our sperm simulations, the average distance of the flagellum the wall is about $3\,a$, and the flagellum rarely comes closer to the wall than $1.5\,a$, we conclude that our

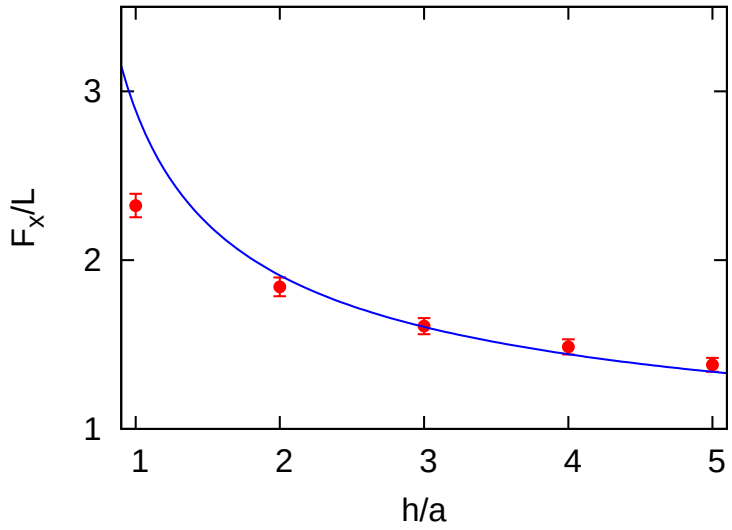

FIG. 5: Drag force F_x/L per unit length (in units of k_BT/a^2), for velocity $U = 0.02\sqrt{k_BT/m}$, as a function of the distance h from a plane wall with no-slip boundary conditions. Symbols (red) indicate simulation results obtained from finite size scaling, the blue solid line shows the theoretical expression (10) without any adjustable parameters.

simulation approach captures near-wall hydrodynamics quantitatively.

---

[1] Ishikawa, T., G. Sekiya, Y. Imai, and T. Yamaguchi. 2007. Hydrodynamic interactions between two swimming bacteria. *Biophys. J.* 93:2217–2225.

[2] Elgeti, J., and G. Gompper. 2008. Hydrodynamics of active mesoscopic systems. *In* NIC Symposium 2008. G. Münster, D. Wolf, and M. Kremer, editors, *NIC series*, volume 39. Neumann Institute for Computing, Jülich. 53–61.

[3] Lamura, A., G. Gompper, T. Ihle, and D. M. Kroll. 2001. Multi-particle-collision dynamics: Flow around a circular and square cylinder. *Europhys. Lett.* 56:319–325.

[4] Gompper, G., T. Ihle, D. M. Kroll, and R. G. Winkler. 2009. Multi-particle collision dynamics – a particle-based mesoscale simulation approach to the hydrodynamics of complex fluids. *Adv. Polym. Sci.* 221:1–87.

[5] Böhmer, M., Q. Van, I. Weyand, V. Hagen, M. Beyermann, M. Matsumoto, M. Hoshi, E. Hildebrand, and U. B. Kaupp. 2005. Ca^{2+} spikes in the flagellum control chemotactic behavior or

sperm. *EMBO J.* 24:2741–2752.

[6] Lighthill, J. L. 1976. Flagellar hydrodynamics. *SIAM Rev.* 18:161–230.

[7] Tirado, M. M., C. L. Martinez, and J. G. de la Torre. 1984. Comparison of theories for the translational and rotational diffusion coefficients of rod-like macromolecules – application to short dna fragments. *J. Chem. Phys.* 81:2047–2052.

[8] Winkler, R. G., K. Mussawisade, M. Ripoll, and G. Gompper. 2004. Rodlike colloids and polymers in shear flow: A multiparticle-collision dynamics study. *J. Phys.: Condens. Matter.* 16:S3941–S3954.

[9] Shack, W. J., C. S. Fray, and T. J. Lardner. 1974. Observations on the hydrodynamics and swimming motions of mammalian spermatozoa. *Bull. Math. Biol.* 36:555–565.

[10] Cox, R. G. 1970. The motion of long slender bodies in a viscous fluid. part 1. general theory. *J. Fluid Mech.* 44:791–810.

[11] Jeffrey, D. J., and Y. Onishi. 1981. The slow motion of a cylinder next to a plane wall. *Q. J. Mech. appl. Math.* XXXIV:129–137.

[12] Götze, I. O., H. Noguchi, and G. Gompper. 2007. Relevance of angular-momentum conservation in mesoscale hydrodynamics simulations. *Phys. Rev. E.* 76:046705 [1–9].

[13] Padding, J. T., and W. J. Briels. 2010. Translational and rotational friction on a colloidal rod near a wall. *J. Chem. Phys.* 132:054511.

Movies

Movie S1. Unconstrained swimming behavior of a sperm cell with chirally asymmetric shape. The sperm structure consists of a spherical head (red), a curved midpiece (yellow - light blue) with preferred curvature $c_0^{(m)} L_m = 1$, and a beating tail (dark blue - light blue). A traveling sinusoidal deformation of the tail generates a forward thrust. The curvature plane of the midpiece is tilted by an angle $\pi/3$ with respect to the beating plane. The helical swimming trajectory is indicated by a pearl necklace of grey beads.

Movie S2. Movie of a symmetric sperm cell (MCE model) approaching a wall. The sperm is released in the bulk fluid and swims on a straight trajectory until it reaches the wall. It remains captured by the wall for the rest of the simulation. It should be noticed that the beating plane is oriented parallel to the wall in the adsorbed state.

Movie S3. Movie of a chirally asymmetric sperm cell (MCE model) approaching a wall. The sperm has a midpiece curvature of $c_0^{(m)} L_m = 1$. The sperm is released in the bulk fluid and swims on a helical trajectory until it reaches the wall. Here, it reorients itself and enters a circular path, which it follows for the rest of the simulation (the trajectory is indicated by a pearl necklace of grey beads). The beating plane is oriented perpendicular to the wall in the adsorbed state.